MOLECULAR AND CELLULAR BIOLOGY, May 2006, p. 3659–3671 Vol. 26, No. 9
0270-7306/06/$08.00+0 doi:10.1128/MCB.26.9.3659–3671.2006

The Retinoblastoma Protein Regulates Pericentric Heterochromatin

Christian E. Isaac,[1,3] Sarah M. Francis,[1,3] Alison L. Martens,[1] Lisa M. Julian,[1,3] Laurie A. Seifried,[1,3] Natalie Erdmann,[4] Ulrich K. Binné,[5] Lea Harrington,[4] Piotr Sicinski,[6] Nathalie G. Bérubé,[2,3] Nicholas J. Dyson,[5] and Frederick A. Dick[1,2,3,5]*

London Regional Cancer Program,[1] Children's Health Research Institute,[2] and Department of Biochemistry[3], University of Western Ontario, London, Ontario, Canada; Campbell Family Institute for Breast Cancer Research, Toronto, Ontario, Canada[4]; Massachusetts General Hospital Cancer Center, Charlestown, Massachusetts[5]; and Dana-Farber Cancer Institute, Boston, Massachusetts[6]

Received 7 October 2005/Returned for modification 9 November 2005/Accepted 3 February 2006

The retinoblastoma protein (pRb) has been proposed to regulate cell cycle progression in part through its ability to interact with enzymes that modify histone tails and create a repressed chromatin structure. We created a mutation in the murine *Rb1* gene that disrupted pRb's ability to interact with these enzymes to determine if it affected cell cycle control. Here, we show that loss of this interaction slows progression through mitosis and causes aneuploidy. Our experiments reveal that while the LXCXE binding site mutation does not disrupt pRb's interaction with the Suv4-20h histone methyltransferases, it dramatically reduces H4-K20 trimethylation in pericentric heterochromatin. Disruption of heterochromatin structure in this chromosomal region leads to centromere fusions, chromosome missegregation, and genomic instability. These results demonstrate the surprising finding that pRb uses the LXCXE binding cleft to control chromatin structure for the regulation of events beyond the G_1-to-S-phase transition.

Deregulated control of cell proliferation is considered to be one of the fundamental characteristics of cancer cells (21). The retinoblastoma protein (pRb) is a key regulator of entry into the cell division cycle and is thought to control proliferation through transcriptional repression of E2F target genes (53). Negative control of gene expression by pRb involves binding to E2F transcription factors. A second, independent interaction between pRb and chromatin-regulating enzymes can further silence gene expression. Most human cancers possess mutations that serve to inactivate pRb function and disrupt transcriptional repression (50).

Chromatin structure plays a key role in the regulation of gene transcription. Eukaryotic cells generate chromatin by winding DNA around histones. Posttranslational modification of histone tails can then "code" regions of chromatin as being accessible for events like transcription or inaccessible to silence gene expression or protect sequences near centromeres and telomeres (6, 30). The Rb family of pocket proteins (pRb, p107, and p130) can interact with a number of enzymes that regulate histone modifications to generate repressive chromatin in transcriptional control (53), telomere length maintenance (19), and centromere function (20). These include deacetylating histones to block transcription (7, 35, 36) and trimethylating histone H3-K9 and histone H4-K20 to establish heterochromatin (20, 40). Direct interaction with histone deacetylases (HDAC1, -2, and -3), H3-K9 methyltransferases (Suv39h1 and -2), and H4-K20 methyltransferases (Suv4-20h1 and -2) are believed to allow pRb to direct these modifications (20, 22, 40). In addition to modifying histone tails, pRb also influences the accessibility of chromatin through interactions with the ATP-dependent helicases BRG1 and Brm (14, 54), as well as DNA methyltransferase 1 (44). The majority of these enzymes interact with pRb through a peptide sequence motif called "LXCXE" that resembles the interaction domain found on viral oncoproteins like HPV E7 (37). Since there are so many enzymes that can interact with pRb in this manner, it is unclear how they are selected to interact with pRb or when their individual activities are important for cell cycle control.

Deregulated gene expression caused by the loss of pRb or its associated chromatin regulators may affect cell cycle control in multiple ways. In addition to defects in G_1 progression, deregulated expression of cyclin E caused by the loss of pRb function has also been observed to lead to aneuploidy and polyploidy (39). Loss of transcriptional control of mitotic regulators, like Mad2, early in the cell cycle can cause defects later in the spindle checkpoint that result in the missegregation of chromosomes (24). Trimethylation of H4-K20 is a mark for silenced heterochromatin that is enriched at pericentric DNA (48). Deficiency in all three pocket proteins disrupts trimethylation of H4-K20 and leads to centromere fusion and genomic instability (20). Together, these reports illustrate that loss of chromatin regulation by pRb may affect processes that are seemingly unrelated, or indirectly related, to changes at the G_1-to-S-phase transition.

Mouse gene-targeting technology provides a way to genetically dissect the mammalian cell cycle. The use of primary fibroblast cultures derived from knockout embryos allows the study of a specific deficiency in an otherwise-normal cell. Primary cultures of mouse embryonic fibroblasts (MEFs) have been the cell type of choice in numerous cell cycle studies (51). Analysis of *Rb1*$^{-/-}$ cells has provided the most definitive evidence for pRb's role in both G_1-to-S-phase regulation and maintenance of DNA content (23, 24, 26, 27, 39). In recent years, it has become clear that compensation can mask the effects of loss-of-function mutations of cell cycle regulators, and this phenomenon represents a major obstacle to identify-

* Corresponding author. Mailing address: Cancer Research Labs, 790 Commissioners Road East, London, Ontario, Canada, N6A 4L6. Phone: (519) 685-8620. Fax: (519) 685-8620. E-mail: fdick@uwo.ca.

ing the true functions of these proteins (51). Studies of the pRb family have shown that the loss of pRb leads to the upregulation of p107 expression, and this change allows p107 to perform new functions in the absence of pRb (28, 45, 47). Since p107 and p130 both contain an LXCXE binding site in their pocket domains, it is unclear whether the phenotypes of *Rb1*$^{-/-}$ cells truly reveal when chromatin regulation by pRb is needed, because p107 and p130 may compensate for the absence of pRb.

To discover when pRb interactions with LXCXE-containing chromatin regulators are important, we generated a mutant strain of mice carrying three amino acid substitutions in the LXCXE binding site of the pocket domain. Cells homozygous for this mutation are distinct from *Rb1*$^{-/-}$ cells in that they contain all three pRb family members, and this may limit the opportunity for compensation for pRb functions by other pocket proteins. The analysis of MEF cultures shows that LXCXE interactions with pRb are essential for H4-K20 trimethylation at pericentric heterochromatin, a defect not found in *Rb1*$^{-/-}$ MEFs. Disruption of pericentric heterochromatin structure leads to centromere fusions in mitosis and missegregation of chromosomes. Our approach provides novel insight into pRb function, because it reveals a role for pRb that was previously concealed by functional compensation.

MATERIALS AND METHODS

Gene targeting and cell culture. Embryonic stem (ES) cells were cultured, transfected, and selected as described previously (52). Correctly targeted cells were identified by Southern blotting and injected into blastocysts to generate chimeric mice. Male chimeras were bred to black-coated *EIIa-cre* transgenic female mice to delete the PGK-neo^r cassette (32). F_1 progeny were intercrossed, and *Rb1*$^{\Delta L/+}$ mice without the *EIIa-cre* transgene were used for the experiments in this study. Genotyping methods and primer sequences are available on request. Wild-type and *Rb1*$^{\Delta L/\Delta L}$ cultures were derived from matched littermates, and all experiments were carried out using passage 3, 4, or 5 MEFs that were generated as described by Hurford et al. (28). Cultures of *Rb1*$^{-/-}$ cells, and littermate controls, were also generated by the same methods. All animals were housed and handled as approved by the Canadian Council on Animal Care.

Protein expression and interaction analysis. Protein extracts were generated by lysing cells in RIPA buffer. Approximately 40 μg of total cellular proteins were resolved in each lane by sodium dodecyl sulfate-polyacrylamide gel electrophoresis, transferred to membranes, and probed using standard methods. For histone modification blots, cells were lysed in NI buffer (15 mM Tris, pH 7.5, 60 mM KCl, 15 mM NaCl, 300 mM sucrose, 1 mM $CaCl_2$, 1 mM dithiothreitol, and 0.5% NP-40), and the nuclear pellets were resuspended in RIPA buffer. Samples were normalized for histone content, separated by 15% sodium dodecyl sulfate-polyacrylamide gel electrophoresis, and transferred to membranes for immunodetection. Proteins were detected using the following antibodies: pRb (G3-245; BD-Pharmingen), p107 (sc-318; Santa Cruz), p130 (sc-317; Santa Cruz), β-actin (A-2066; Sigma), RBP1 (LY11), Sin3A (06-913; Upstate), CtBP1 (clone 3; BD Biosciences), HDAC1 (sc-6298; Santa Cruz), HDAC2 (sc-6296; Santa Cruz), RbAp46 (sc-8272; Santa Cruz), E2F1 (KH95), NF-κB p65 (sc-109; Santa Cruz), Mad2 (clone 48; BD Biosciences), trimethyl-H4-K20 (07-463; Upstate), and histone H4-pan (05-858; Upstate).

Glutathione *S*-transferase (GST) "pull-down" experiments (see Fig. 2A) were carried out essentially as described by Dick et al. (12), and bound proteins were analyzed by Western blotting as described above. GST-Rb pull-downs (see Fig. 2C) were carried out as described by Näär et al. using HeLa nuclear extracts as a source of protein (38). All GST-Rb constructs contained the large pocket domain of pRb (amino acids 379 to 928). GST–Suv4-20h1 and -2 pull-downs (see Fig. 2D) were performed as described by Gonzalo et al. (20). Briefly, recombinant proteins, or GST as a control, were incubated with whole-cell extracts from MEFs overnight at 4°C in GSE buffer (20 mM Tris, pH 7.5, 150 mM NaCl, 1.5 mM $MgCl_2$, 0.2 mM EDTA, 1 mM dithiothreitol, 0.5% NP-40). Beads were washed with GSE buffer, and bound pRb was detected by Western blotting. Electrophoretic mobility shift assays were performed as described previously (11), and pRb was supershifted with a mouse monoclonal antibody (21C9).

Northern blot analysis. Total cellular RNA was extracted from asynchronous and serum-starved MEFs using Trizol reagent according to the manufacturer's instructions (Invitrogen). RNA was resolved by agarose gel electrophoresis, blotted onto nylon membranes, and cross-linked with a UV light source. Antisense riboprobes labeled with [^{32}P]UTP were generated by T3 polymerase transcription of cDNA fragments cloned into pBluescript. Membranes were blocked, probed, and washed as described by Frolov et al. (18). The membranes were stripped and reprobed with an *ARPP*$_0$ probe to confirm equal loading of lanes.

Cell cycle analysis. Cell cycle analysis was performed by pulse-labeling cells with bromodeoxyuridine (BrdU) (RPN201V1; Amersham Biosciences) according to the manufacturer's instructions for 1 hour prior to harvesting them. The cells were detached from the plates, fixed in ethanol, and immunostained with anti-BrdU antibodies (347580; BD Biosciences), along with propidium iodide (PI) as reported previously (8). Phospho-H3-S10 staining (06-570; Upstate) was performed essentially as described by Taylor (55). Cell populations were analyzed by flow cytometry on a Beckman-Coulter EPICS XL-MCL instrument. Data analysis was carried out using the CXP version 2 software package.

The length of G_1 was measured by arresting cells at confluence, followed by replating them at low density. The cells were pulse-labeled with BrdU for 30 min every 2 hours and processed for flow cytometry. S-phase and G_2/M progression was measured by releasing cells from confluence into media containing 4 μg/ml of aphidicolin (A0781; Sigma). After 10 h, the cells were washed and fed with fresh medium to release them into S phase. Spindle checkpoint function was determined by culturing fibroblasts in the presence of 150 nM nocodazole or dimethyl sulfoxide before staining them with propidium iodide and phospho-H3-S10 and analysis by flow cytometry.

ChIP. MEFs at 80% confluence were cross-linked with 1% formaldehyde in medium for 10 min at room temperature (41). Cross-linking was stopped with 125 mM glycine, and nuclear extracts were prepared for chromatin immunoprecipitation (ChIP) using the procedures described by Aparicio et al. (3). Chromatin was sonicated to yield an average DNA fragment size of 350 base pairs (range, 100–850 bp) as analyzed on agarose gels. Chromatin (400 μg) was used in immunoprecipitations with 3Me-H4-K20-specific and histone H4-pan antibodies or rabbit immunoglobulin G as a control. Cross-links were reversed and immunoprecipitated, and input DNA (40 μg fragmented chromatin) was purified by phenol-chloroform extraction before being analyzed by conventional and real-time PCR. Primer pairs to amplify major satellite repeats were as described by Lehnertz et al. (34) and produced a ladder of products 74, 308, and 542 bp in length. PCR products were resolved on 2.5% agarose gels containing ethidium bromide, analyzed under UV light, and presented as negative images. Real-time quantitative PCR was carried out with iQ SYBR Green Supermix on a PTC-200 Thermal Cycler equipped with a Chromo 4 Continuous Fluorescence Detector, and data were analyzed using the Opticon Monitor 3.1 software package (Bio-Rad).

Fluorescence microscopy and karyotyping. MEF cultures were fixed and stained with antibodies against trimethylated H4-K20 (07-463; Upstate), monomethylated H3-K27 (07-448; Upstate), and trimethylated H3-K9 (07-442; Upstate), following methodologies outlined by Zhao et al. (59). For analysis of lagging chromosomes, MEF cultures were synchronized with aphidicolin as described above before fixation and staining with DAPI (4′,6′-diamidino-2-phenylindole). For karyotypic analysis, MEFs were treated with 50 ng/ml Karyomax Colcemid (Invitrogen) for 3 hours, harvested, swollen in 75 mM KCl, and fixed in 3:1 methanol-acetic acid before being dropped onto standard microscope slides. The slides were chemically aged as described by Herrera et al. (25), and centromere fluorescent in situ hybridization (FISH) analysis of metaphase spreads was performed using a centromere-specific probe constructed by labeling PCR-amplified major satellite repeats with fluorescein-12-dUTP (R0101; Fermentas). The slides were hybridized using a protocol modified from Dorin et al. (13). Telomere FISH experiments utilized a Cy3-PNA probe and were carried out essentially as described by Zijlmans et al. (60). H4-K20 trimethyl staining of unfixed metaphase chromosomes was performed as detailed by Aagaard et al. (1).

RESULTS

The *Rb1*$^{\Delta LXCXE}$ protein is defective for interactions with chromatin regulators. To examine the importance of pRb's interaction with chromatin regulators in vivo, we used gene targeting to create point mutations in the LXCXE binding site of the endogenous mouse *Rb1* gene. Previous studies had revealed that replacing I753, N757, and M761 with alanine blocks LXCXE interactions with human pRb (12). The murine equivalent of this mutant allele (I740A, N744A, M748A) is

called $Rb1^{\Delta LXCXE}$ and, for brevity, is referred to as $Rb1^{\Delta L}$ throughout this report. The gene-targeting strategy used to create $Rb1^{\Delta L}$ is outlined in Fig. 1A. Correctly targeted ES clones were identified by Southern blotting as shown in Fig. 1B. Chimeric mice were bred to black-coated *EIIa-cre* transgenic females with a mixed 129 and C57BL/6 background. Correct excision of the PGK-neo^r cassette was detected by PCR of tail DNA from F_1 progeny (Fig. 1C). To further confirm the correct introduction of only the desired mutations, exon 22 from $Rb1^{\Delta L/\Delta L}$ homozygous mutant mice was PCR amplified and sequenced (data not shown). $Rb1^{\Delta L/\Delta L}$ mutants are viable and fertile in a mixed 129 and C57BL/6 background and were obtained at nearly the expected Mendelian ratio (Fig. 1D). Our goal was to evaluate the fundamental need for pRb to interact with chromatin-regulating enzymes in cell cycle control. For this reason, we established embryonic fibroblast cultures from $Rb1^{\Delta L/\Delta L}$ mice and investigated how cell cycle regulation was altered by this mutation.

Analysis of proliferating $Rb1^{\Delta L/\Delta L}$ fibroblasts confirmed that the level of the mutant pRb$^{\Delta L}$ protein is equivalent to that seen in wild-type cells and showed that the related p107 and p130 pocket proteins also had unchanged levels of expression (Fig. 2A). The $Rb1^{\Delta L}$-encoded protein was unable to bind to GST-E7, a known LXCXE-dependent interaction (Fig. 2A). In contrast, electrophoretic mobility shift assays indicated that the pRb$^{\Delta L}$ protein interacted with E2F transcription factors in a manner that was indistinguishable from that of the wild type (Fig. 2B). Pull-down experiments confirmed that GST-pRb$^{\Delta L}$ was defective for interaction with a series of LXCXE-dependent pRb-binding proteins, including RBP1, Sin3, CtBP, HDAC1, HDAC2, and RbAp46 (Fig. 2C), and this mutation abrogated the ability of GST-pRb to recruit HDAC catalytic activity from nuclear extracts (data not shown). In light of the findings described below, we also examined pRb's ability to interact with GST–Suv4-20h1 and -2 proteins, two non-LXCXE-containing histone methyltransferases. Figure 2D shows that both pRb and the pRb$^{\Delta L}$ mutant proteins are able to bind to Suv4-20h enzymes.

Chromatin regulation by pRb has been shown to facilitate transcriptional repression. Since disruption of LXCXE interactions between pRb and chromatin regulators was predicted to derepress transcription, we compared the expression of E2F-regulated genes in wild-type, $Rb1^{-/-}$, or $Rb1^{\Delta L/\Delta L}$ cells. $Rb1^{\Delta L/\Delta L}$ cells have noticeably elevated levels of expression of E2F target genes when synchronized in G_0 by serum starvation (Fig. 2E), a condition in which E2F-regulated genes are known to be derepressed in the absence of pRb (28). However, the mRNA levels of these genes were not altered in asynchronously growing $Rb1^{\Delta L/\Delta L}$ cultures (Fig. 2E), suggesting that repression mediated by LXCXE interactions does not greatly limit the expression of these genes in the total population once cells are proliferating. This supports the observation that p107 expression is not increased in growing cells (Fig. 2A). From these experiments, we conclude that disruption of active repression by pRb does not significantly affect E2F transcription in proliferating cells.

These results confirm that pRb$^{\Delta L}$ is expressed normally, interacts with E2Fs, and is unable to actively repress transcription of E2F targets. Thus, the $Rb1^{\Delta L}$ protein possesses the biochemical characteristics necessary to study the role of LXCXE-dependent interactions with pRb in isolation from its other activities. If pRb interactions with LXCXE-containing chromatin regulators are needed for cell cycle control, these functions should be revealed as cell cycle defects in the $Rb1^{\Delta L/\Delta L}$ MEF cultures.

Mitotic defects in $Rb1^{\Delta L/\Delta L}$ fibroblasts. To discover when LXCXE-dependent interactions with pRb may be required, we compared the cell cycle distributions of proliferating wild-type, $Rb1^{-/-}$, and $Rb1^{\Delta L/\Delta L}$ MEFs. The proportion of cells in each phase of the cell cycle was determined by flow cytometry of PI- and BrdU-stained cells. $Rb1^{-/-}$ cultures have been shown to exhibit a decreased abundance of G_0/G_1 cells and an increase in S phase as a result of premature entry into the cell cycle (27). Presumably, acceleration through G_1 is caused by deregulation of E2F target genes. Since E2F targets are elevated only in quiescent $Rb1^{\Delta L/\Delta L}$ cells and not in proliferating cultures (Fig. 2D), we were not surprised to find that the $Rb1^{\Delta L/\Delta L}$ mutant MEFs exhibited no change in their S-phase populations compared to the wild type (Fig. 3A). Instead, these cultures had a slightly smaller G_0/G_1 population and an elevated number of G_2/M-phase cells (Fig. 3A). Similar results were obtained using six different pairs of wild-type and mutant fibroblasts prepared in parallel from sibling embryos. This finding was confirmed using MEFs from a second colony of mice derived from an independent ES clone. Throughout these experiments, we observed an increase in G_2/M and the appearance of aneuploid cells with greater than 4N DNA in the $Rb1^{\Delta L/\Delta L}$ cultures (Fig. 3A and 4B).

The decrease in G_0/G_1 abundance and elevation of G_2/M cells in $Rb1^{\Delta L/\Delta L}$ fibroblasts shown in Fig. 3A suggests either a slightly early entry into S phase and an unrelated delay later in the cell cycle or a slowed progression through G_2/M that creates a diminished return to G_1. To distinguish between these possibilities, we synchronized wild-type and $Rb1^{\Delta L/\Delta L}$ mutant fibroblasts by contact inhibition and induced cell cycle reentry by reseeding them at low density. $Rb1^{\Delta L/\Delta L}$ mutant and wild-type cells were found to transit through G_1 and reach their peaks of DNA synthesis at the same time (Fig. 3B), suggesting that the mutant cells do not prematurely enter S phase. Premature S-phase entry often results in a smaller cell size because the cells have insufficient time to grow (31). Forward-scatter analysis of G_1 cells from Fig. 3A indicated that $Rb1^{\Delta L/\Delta L}$ cells were comparable in size to wild-type cells (Fig. 3C) and lacked the size defect that is evident with $Rb1^{-/-}$ MEFs (27). Together, these results indicate that $Rb1^{\Delta L/\Delta L}$ MEFs lack the shortened G_1 that is characteristic of $Rb1^{-/-}$ MEFs.

To investigate the impact of the $Rb1^{\Delta L}$ mutation on S-, G_2-, and M-phase progression, cells were synchronized at the beginning of S phase with aphidicolin and released from arrest. PI-BrdU staining and PI–phospho-H3-S10 staining, followed by flow cytometry, were used to measure transit through S phase and to visualize the onset of mitosis. In these assays, $Rb1^{\Delta L/\Delta L}$ MEFs were indistinguishable from wild-type cells (data not shown), indicating that transit through S phase and G_2 was unaltered. This suggested that the defect in $Rb1^{\Delta L/\Delta L}$ cells likely occurs after H3-S10 phosphorylation diminishes in metaphase (55). To test this, synchronized cultures were stained and examined for defects in mitosis. The DAPI-stained cells in Fig. 4A illustrate mitotic abnormalities that are typical of $Rb1^{\Delta L/\Delta L}$ cells. Both mutant images show lagging chromosomes that are indicative of nondisjunction of sister chromatids

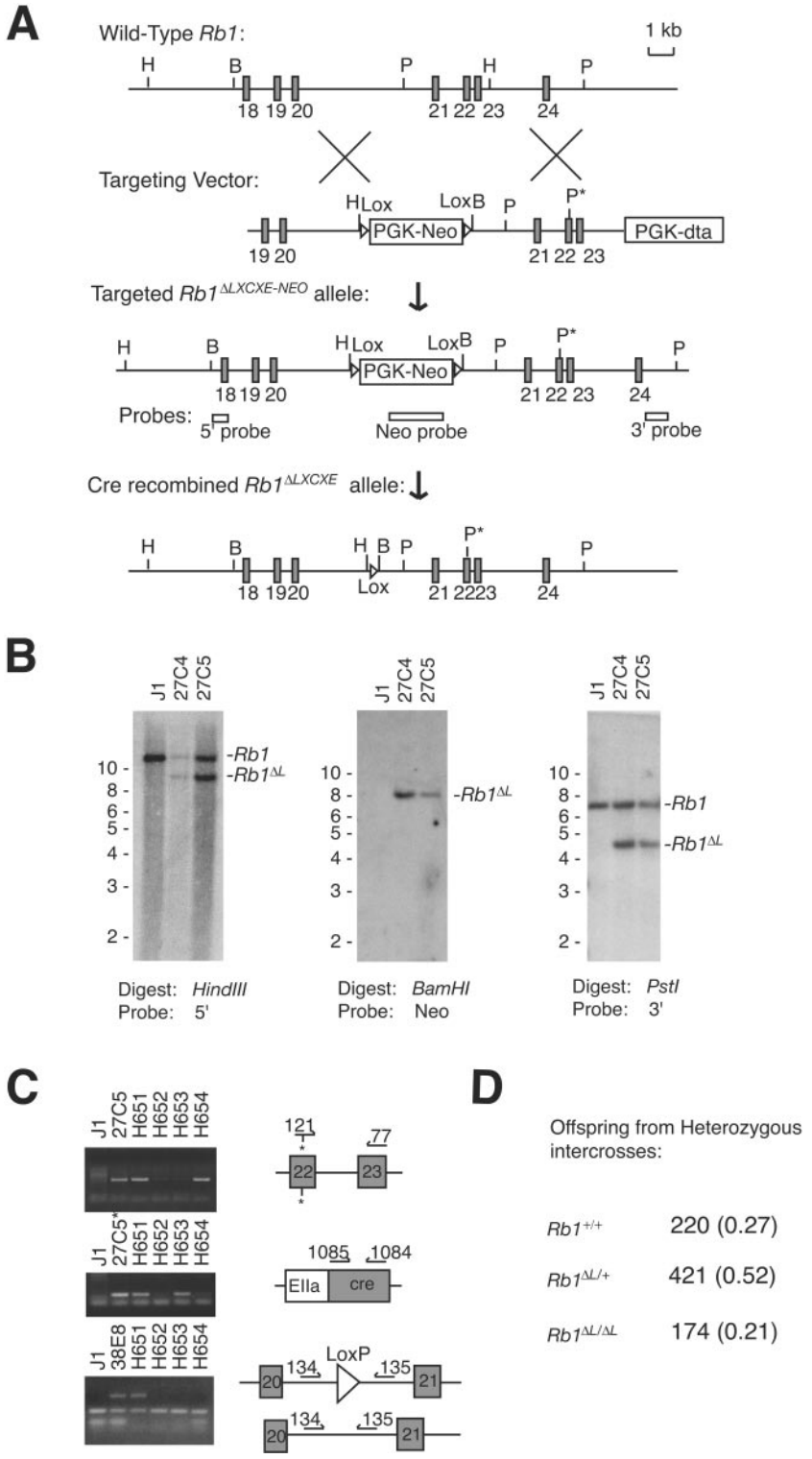

FIG. 1. Generation of the $Rb1^{\Delta LXCXE}$ mutant mouse strain. (A) The genomic structure of the B-pocket coding region of *Rb1* is shown at the top. The targeting vector contained a LoxP-flanked PGK-neo^r cassette inserted into intron 20 and the ΔLXCXE mutations of I740A, N744A, and M748A in exon 22 (marked by a silent PstI site). Homologous recombination resulted in the $Rb1^{\Delta LXCXE\text{-}NEO}$ allele that is diagrammed in the middle. The locations of probes used for Southern blotting are shown (H, HindIII; B, BamHI; P, PetI; P*, the PstI site that marks our mutation). The correctly recombined $Rb1^{\Delta LXCXE}$ allele was generated by breeding chimeric male mice with a Cre-expressing transgenic strain, and the structure of a correctly excised allele is shown at the bottom. (B) Southern blots of representative targeted ES clones are shown, along with DNA from the untargeted J1 cells. Restriction enzymes used to digest genomic DNA and the probes that were used to hybridize to each blot are shown below the autoradiographs. (C) PCR detection of the ΔLXCXE mutations in exon 22, presence of the *EIIa-cre* transgene, and correct deletion of the PGK-neo^r cassette are shown. Ethidium bromide-stained gels demonstrate amplification of sequences from control ES cell DNA and tails from F_1 founders. The sequence of primer 121 anneals specifically to the altered sequence in exon 22 of $Rb1^{\Delta L}$. The asterisk next to 27C5 indicates that this DNA sample was supplemented with pMC1-cre to serve as a positive control. Clone 38E8 is an ES line that was generated by transfection with pMC1-cre to delete the neo^r marker and also serves as a positive control. (D) The genotypes of offspring resulting from $Rb1^{\Delta L/+}$ crosses are shown, with genotype frequencies in brackets.

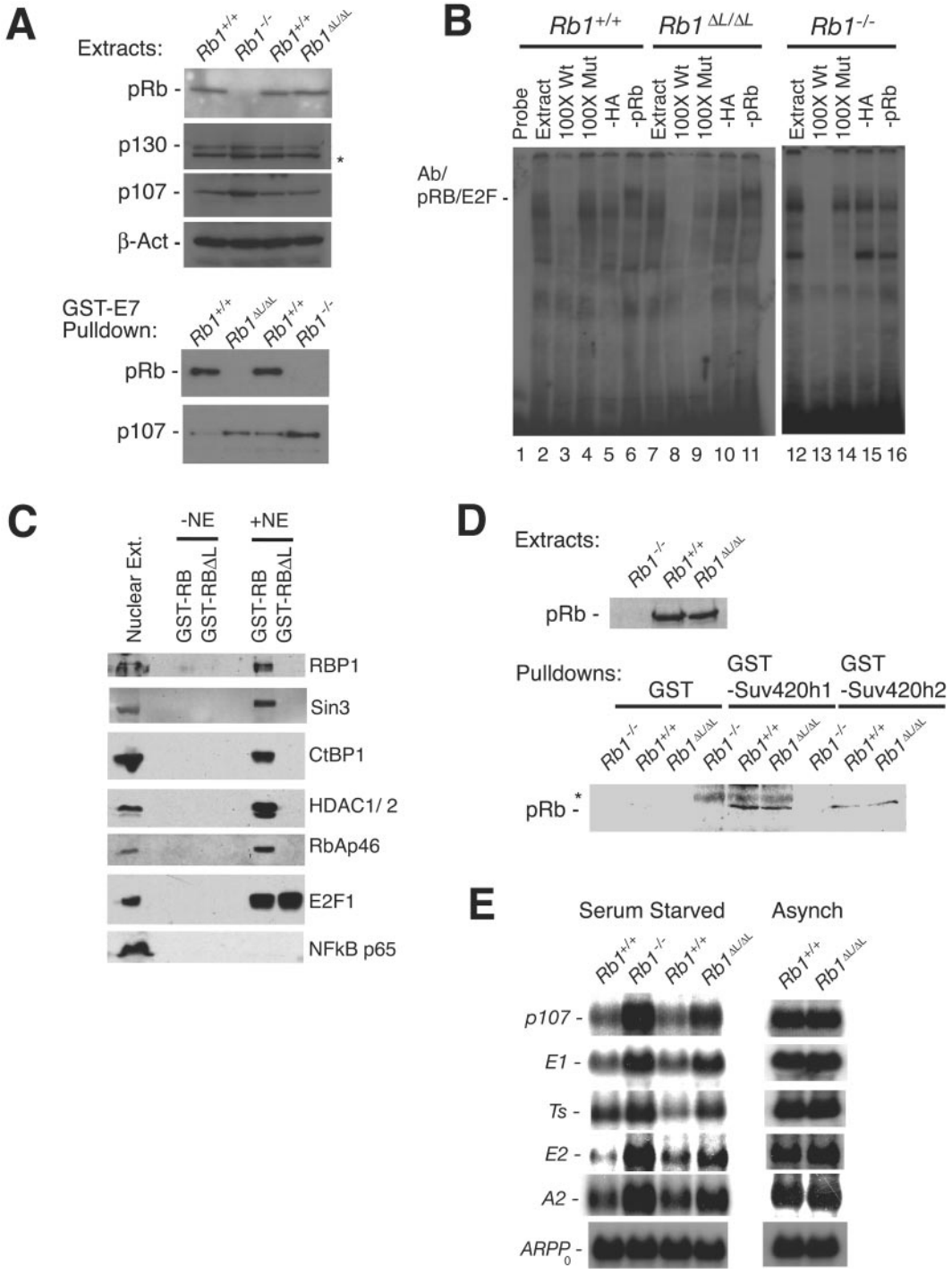

FIG. 2. The $Rb1^{\Delta L}$-encoded protein fails to interact with chromatin-regulating factors and is defective for transcriptional repression. (A) pRb, p107, and p130 protein expression levels were measured in wild-type, $Rb1^{\Delta L/\Delta L}$, and $Rb1^{-/-}$ MEFs by Western blotting (top), and the ability of GST-E7 to interact with pocket proteins was tested in GST pull-down assays and detected by Western blotting (bottom). The asterisk denotes a cross-reactive band in p130 blots. (B) The ability of $pRb^{\Delta L}$ to interact with E2F transcription factors was detected by electrophoretic mobility shift assay. Extracts from wild-type, $Rb1^{\Delta L/\Delta L}$, and $Rb1^{-/-}$ cells were incubated with a radiolabeled double-stranded DNA oligonucleotide containing a consensus E2F binding site. Gel shift complexes were competed with unlabeled wild-type and mutant oligonucleotides (lanes 3, 4, 8, 9, 13, and 14). Complexes containing pRb and E2Fs were identified by supershifting with an α-pRb monoclonal antibody (lanes 6, 11, and 16). (C) The identities of proteins coisolated with GST-Rb from nuclear extracts in an LXCXE binding cleft-dependent manner were determined by Western blotting. Nuclear extract is abbreviated as NE. (D) GST-Suv4-20h1 and -2 proteins were used to coprecipitate pRb from wild-type, $Rb1^{\Delta L/\Delta L}$, and $Rb1^{-/-}$ extracts. Western blots of input and precipitated protein levels are shown. An asterisk denotes background caused by the high-molecular-weight GST-Suv4-20h1 protein. (E) Northern blots were performed on RNA extracted from serum-starved or proliferating MEFs to assess expression of E2F target genes. The blots were probed to quantify message levels for *p107*, *Cyclin E1*, *Thymidylate synthase*, *Cyclin E2*, *Cyclin A2*, and $ARPP_0$ (loading control). Asynch, asynchronous.

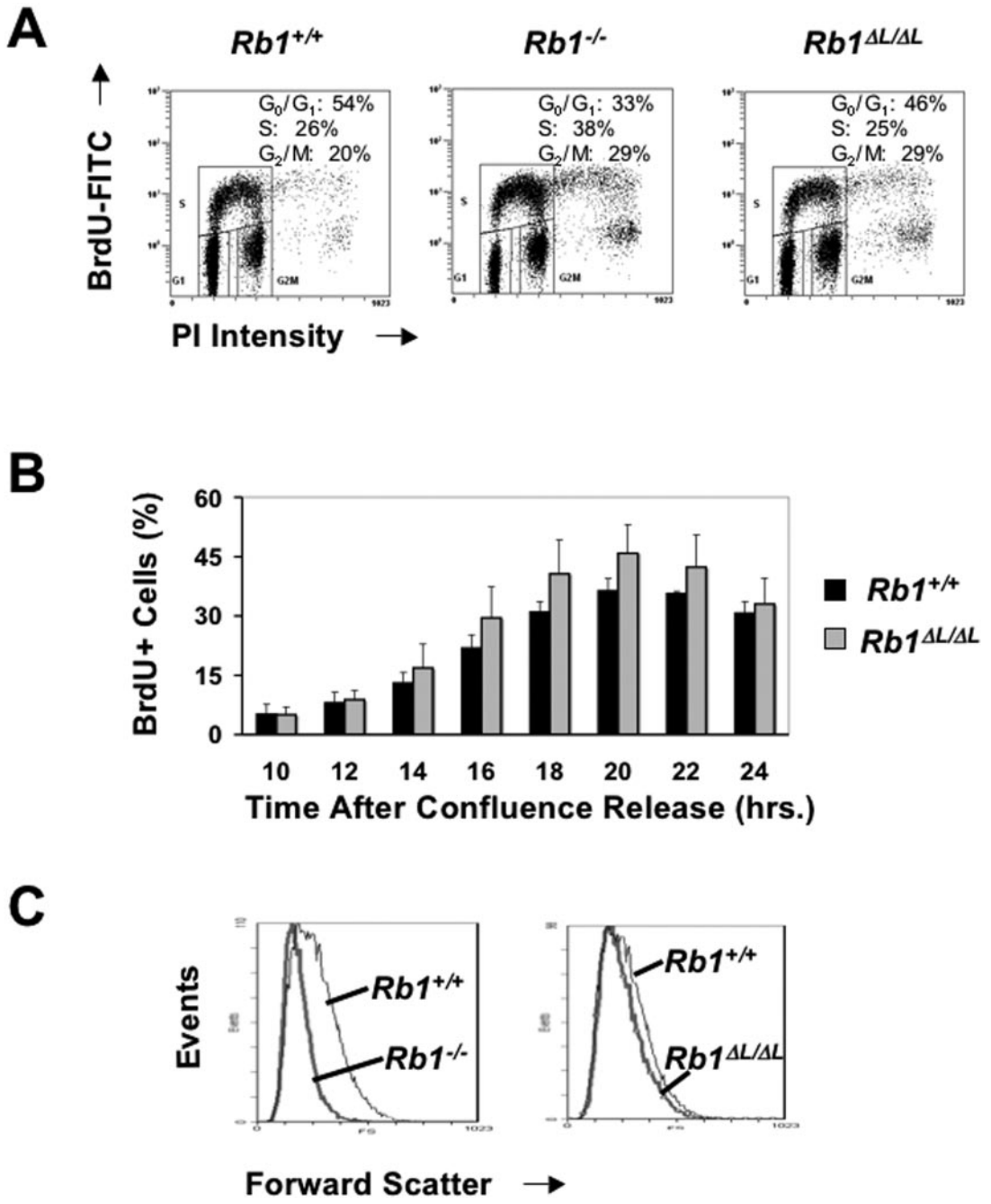

FIG. 3. G_1 progression in $Rb1^{\Delta L/\Delta L}$ MEFs. (A) Actively proliferating MEF cultures were pulse-labeled with BrdU, processed for flow cytometry, and analyzed for propidium iodide and BrdU staining. The proportion of cells in each phase of the cell cycle is indicated for each genotype. (B) The relative lengths of G_1 in $Rb1^{\Delta L/\Delta L}$ and wild-type cells were compared by replating confluent cultures at low density and pulse-labeling them with BrdU at the indicated time points. The percentage of cells incorporating BrdU is shown for three independent experiments. (C) Forward-scatter analysis of the G_1 cells in panel A was used to compare the relative sizes of cells from the different *Rb1* genotypes. The error bars indicate 1 standard deviation from the mean.

during anaphase. Lagging chromosomes are detectable in one-third of all $Rb1^{\Delta L/\Delta L}$ cells during anaphase (Fig. 4A). $Rb1^{\Delta L/\Delta L}$ cultures display an increased percentage of cells with greater than 4N DNA content compared to wild-type MEFs, suggesting that $Rb1^{\Delta L/\Delta L}$ fibroblasts have difficulty completing mitosis and consequently become aneuploid (Fig. 4B). This analysis confirms that $Rb1^{\Delta L/\Delta L}$ fibroblasts have defects that prevent normal progression through mitosis.

Previous reports have demonstrated that the loss of *Rb1* deregulates expression of Mad2. This increase in Mad2 hyperactivates the spindle checkpoint, altering progression through mitosis and resulting in genomic instability (24). To investigate

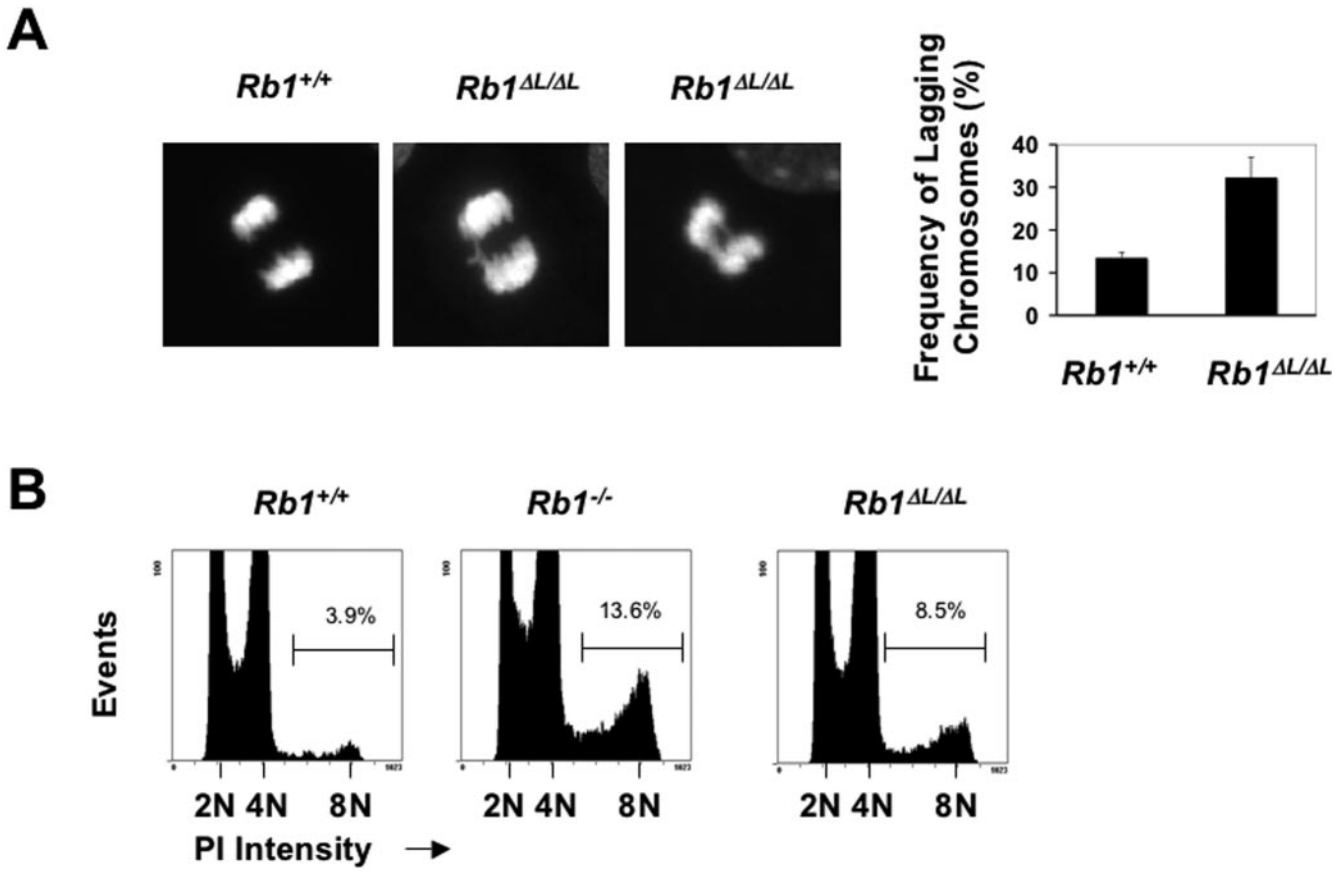

FIG. 4. Mitotic defects in $Rb1^{\Delta L/\Delta L}$ MEFs. (A) DAPI-stained mitotic figures from wild-type and $Rb1^{\Delta L/\Delta L}$ cells are shown. The percentage of mitoses with lagging chromosomes was tabulated for at least 100 anaphases in each of three independent experiments. (B) Propidium iodide-stained cells were analyzed by flow cytometry for cells with greater than 4 N DNA content to identify aneuploid cells. The percentages of cells in this category are indicated above the bars. The error bars indicate 1 standard deviation from the mean.

whether a change in Mad2 expression might underlie the defects seen in $Rb1^{\Delta L/\Delta L}$ cells, we examined Mad2 levels. Mad2 expression in $Rb1^{\Delta L/\Delta L}$ cells is similar to that in the wild type, and $Rb1^{\Delta L/\Delta L}$ cells lack the dramatic increase in Mad2 expression that is evident in $Rb1^{-/-}$ cells (Fig. 5A). As a further test of this model, we investigated whether the spindle checkpoint is active in $Rb1^{\Delta L/\Delta L}$ cells. In mouse cells, adaptation to the spindle checkpoint occurs rapidly and prevents a robust accumulation of cells with condensed chromatin (43). To characterize this transient checkpoint, we utilized a known mitotic marker, phospho-H3-S10, to identify mitotically arrested cells (55). A time course of nocodazole treatment revealed that $Rb1^{\Delta L/\Delta L}$ mutant fibroblasts accumulated and slipped through the spindle checkpoint in a manner that was similar to that of the wild-type controls (Fig. 5B). Since, $Rb1^{\Delta L/\Delta L}$ cells have relatively normal levels of Mad2 and an intact spindle checkpoint, their mitotic defects are unlikely to be attributable to the effects of Mad2 regulation.

pRb regulates pericentric heterochromatin. To better understand the defects in anaphase, we decided to analyze the events that precede them in metaphase. To accomplish this, we examined metaphase chromosome spreads from $Rb1^{\Delta L/\Delta L}$ cells, and these suggested an explanation for the lagging chromosomes shown in Fig. 4. These metaphase spreads frequently contained what appeared to be joined centromeres connecting chromosome pairs (Fig. 6A, middle). This type of abnormality was rarely detected in the wild-type and $Rb1^{-/-}$ negative controls (Fig. 6A). In order to quantify these chromosome fusions, the numbers of touching or shared centromeres found in each mitotic spread from 35 wild-type cells, 35 $Rb1^{\Delta L/\Delta L}$ mutants, and 35 $Rb1^{-/-}$ knockouts were determined. The histogram in Fig. 6B reveals that metaphase spreads from $Rb1^{\Delta L/\Delta L}$ mutants often had more chromosome fusions than either the wild type or $Rb1^{-/-}$. This difference is statistically significant using a χ^2 test ($P < 0.001$). Since mouse chromosomes are acrocentric and have very short p arms, the above-mentioned analysis does not distinguish centromere fusions that create "butterfly" chromosomes from Robertsonian fusions that involve end-to-end joining through telomeres in the p arm. To distinguish between these possibilities, we stained chromosome spreads with FISH probes that were specific for major satellite sequences near the centromere and telomere repeats. Typical staining patterns of fused chromosomes are shown in Fig. 6C. The major satellite probe revealed a clear joining in the centromere region. Telomere staining routinely showed the existence of at least three individual telomere ends. One of these telomeres was repeatedly more brightly stained and was often oblong (Fig. 6C), suggesting that two of the telomeres were very closely spaced

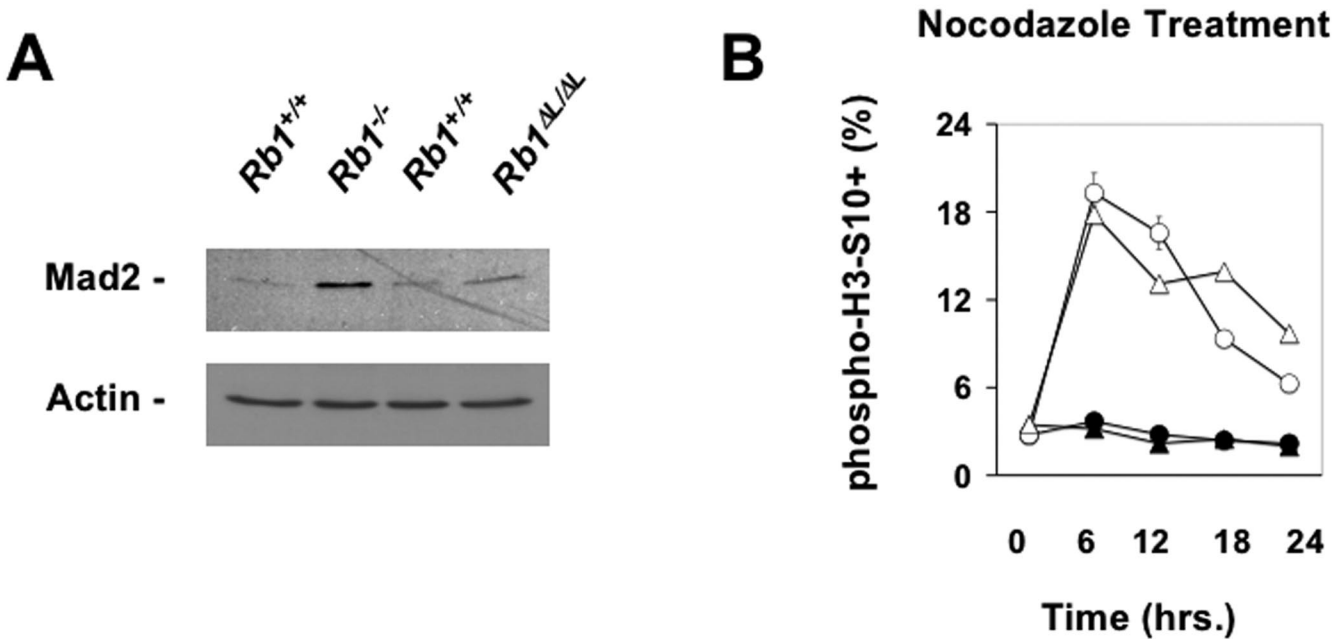

FIG. 5. The spindle checkpoint is unaffected by the $Rb1^{\Delta L}$ mutation. (A) Mad2 expression levels in wild-type, $Rb1^{-/-}$, and $Rb1^{\Delta L/\Delta L}$ fibroblasts were measured by Western blotting. (B) Wild-type and $Rb1^{\Delta L/\Delta L}$ MEFs were cultured in the presence of nocodazole (open symbols) or dimethyl sulfoxide (filled symbols) for the indicated periods of time before being processed for flow cytometry and analyzed for phospho-H3-S10 staining. The circles and triangles indicate wild-type and $Rb1^{\Delta L/\Delta L}$ MEFs, respectively. The error bars indicate 1 standard deviation from the mean.

or possibly joined. We did not observe any end-to-end fusions through signal-free ends on either the p or q arms of chromosomes from $Rb1^{\Delta L/\Delta L}$ cells. Since triple-knockout cells also have elongated telomeres (19), we also measured telomere length in $Rb1^{\Delta L/\Delta L}$ MEFs by Q-FISH. Our measurements revealed that $Rb1^{\Delta L/\Delta L}$ telomeres may be elongated compared with the wild type (data not shown). From these experiments, we conclude that telomeres appear to be stable in $Rb1^{\Delta L/\Delta L}$ cells, and our experimental evidence indicates that chromosome fusions in $Rb1^{\Delta L/\Delta L}$ cells occur through centromeres.

The similarity between our centromere fusion phenotype and that reported for triple-knockout cells lacking all three pRb family proteins (20) prompted us to investigate chromatin structure in pericentric regions. H4-K20 trimethylation, H3-K27 monomethylation, and H3-K9 trimethylation are histone tail modifications that have been shown to be concentrated in pericentric heterochromatin (48). We examined these modifications in interphase nuclei by immunofluorescence microscopy to determine if any of them were altered in $Rb1^{\Delta L/\Delta L}$ MEFs. The degree of colocalization of histone tail modifications with DAPI-rich centromeres in interphase nuclei allowed us to examine this heterochromatin domain. This analysis revealed that only H4-K20 trimethylation is reduced in $Rb1^{\Delta L/\Delta L}$ cells relative to the wild type or $Rb1^{-/-}$ controls (Fig. 7A and data not shown). Analysis of H4-K20 trimethylation of metaphase chromosomes further revealed that pericentric heterochromatin from $Rb1^{\Delta L/\Delta L}$ chromosomes is depleted of this modification but $Rb1^{-/-}$ chromosomes resemble the wild type (Fig. 7A). In addition to our microscopic analysis, we also performed chromatin immunoprecipitations to detect levels of major satellite sequences in H4-K20 trimethyl-specific immunoprecipitations. Rabbit immunoglobulin G and modification-insensitive H4-pan antibodies were used as negative and positive controls, respectively. ChIPs performed with 3Me-H4-K20-specific antibodies revealed that pericentric heterochromatin from $Rb1^{\Delta L/\Delta L}$ cells had less of this modification than wild-type and $Rb1^{-/-}$ cells (Fig. 7B). To further substantiate this result, we also utilized real-time PCR to quantify the amount of chromatin precipitated by 3Me-H4-K20 antibodies. These experiments also demonstrated a significant reduction in chromatin precipitated by 3Me-H4-K20 antibodies from $Rb1^{\Delta L/\Delta L}$ fibroblasts ($P < 0.001$) (Fig. 7C). Taken together, these experiments reveal a defect in H4-K20 trimethylation in $Rb1^{\Delta L/\Delta L}$ cells.

To gauge how widespread the reduction in H4-K20 trimethylation was, we also performed Western blots on total histones from wild-type, $Rb1^{\Delta L/\Delta L}$, and $Rb1^{-/-}$ MEFs. We found that total levels of trimethylated H4-K20 appeared relatively uniform across the three genotypes tested (data not

FIG. 6. Centromere fusions between $Rb1^{\Delta L/\Delta L}$ chromosomes. (A) Representative DAPI-stained chromosome spreads for wild-type, $Rb1^{\Delta L/\Delta L}$, and $Rb1^{-/-}$ are shown. Chromosomes that are joined at the centromere are indicated by an arrow. (B) The number of centromere fusions per metaphase spread is plotted as a frequency histogram; 35 metaphase spreads were examined for each genotype. (C) Centromere and telomere FISH analyses of chromosome fusions. Metaphase chromosome spreads were hybridized with major satellite and telomere probes to visualize their locations in joined chromosomes. The arrow in the leftmost panel indicates a centromere fusion, while the arrow on the right locates the p-arm telomeres nearest to the fusion point.

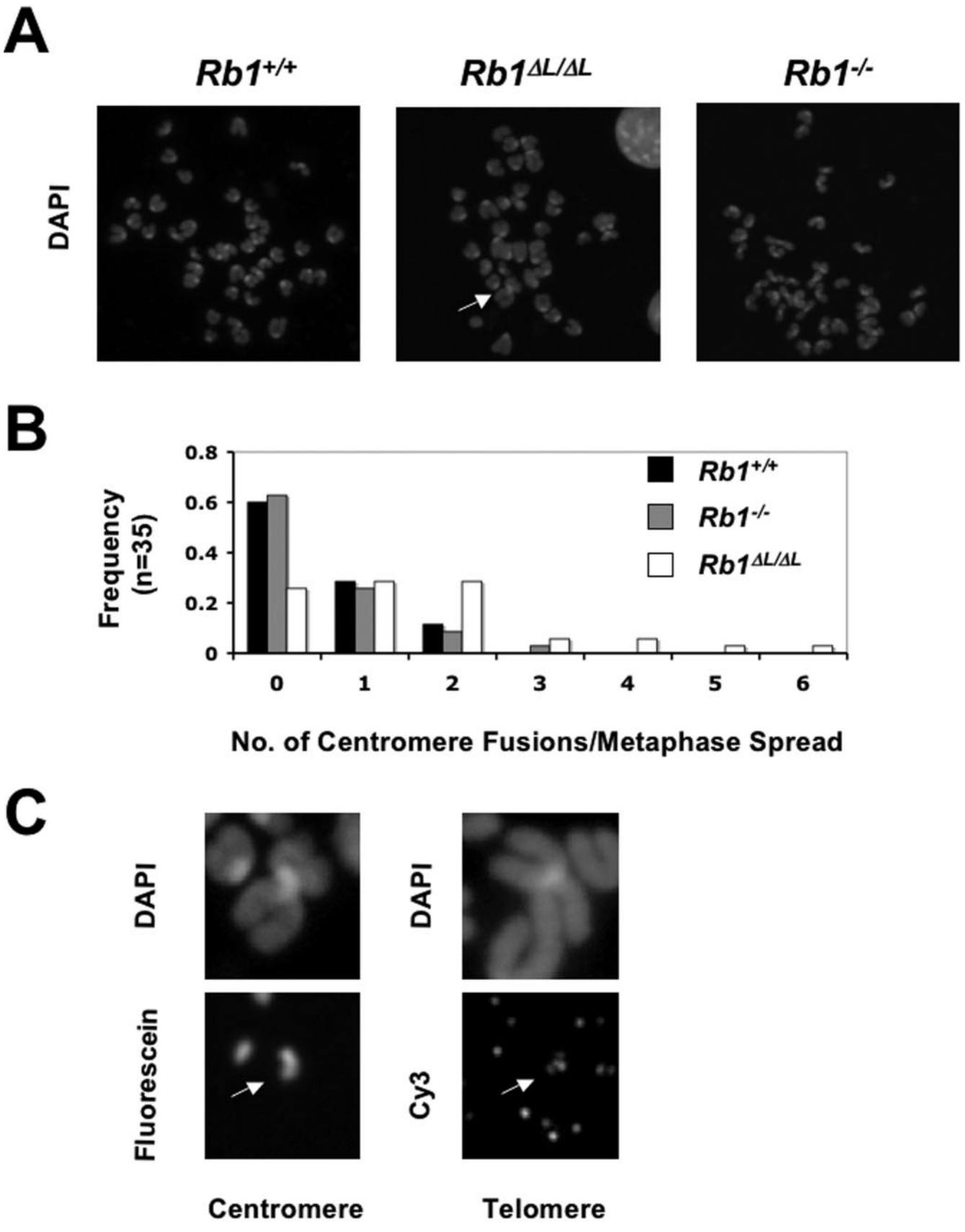
A
Rb1+/+
Rb1ΔL/ΔL
Rb1-/-
DAPI
B
Frequency (n=35)
0.8
0.6
0.4
0.2
0
Rb1+/+
Rb1-/-
Rb1ΔL/ΔL
0
1
2
3
4
5
6
No. of Centromere Fusions/Metaphase Spread
C
DAPI
DAPI
Fluorescein
Cy3
Centromere
Telomere

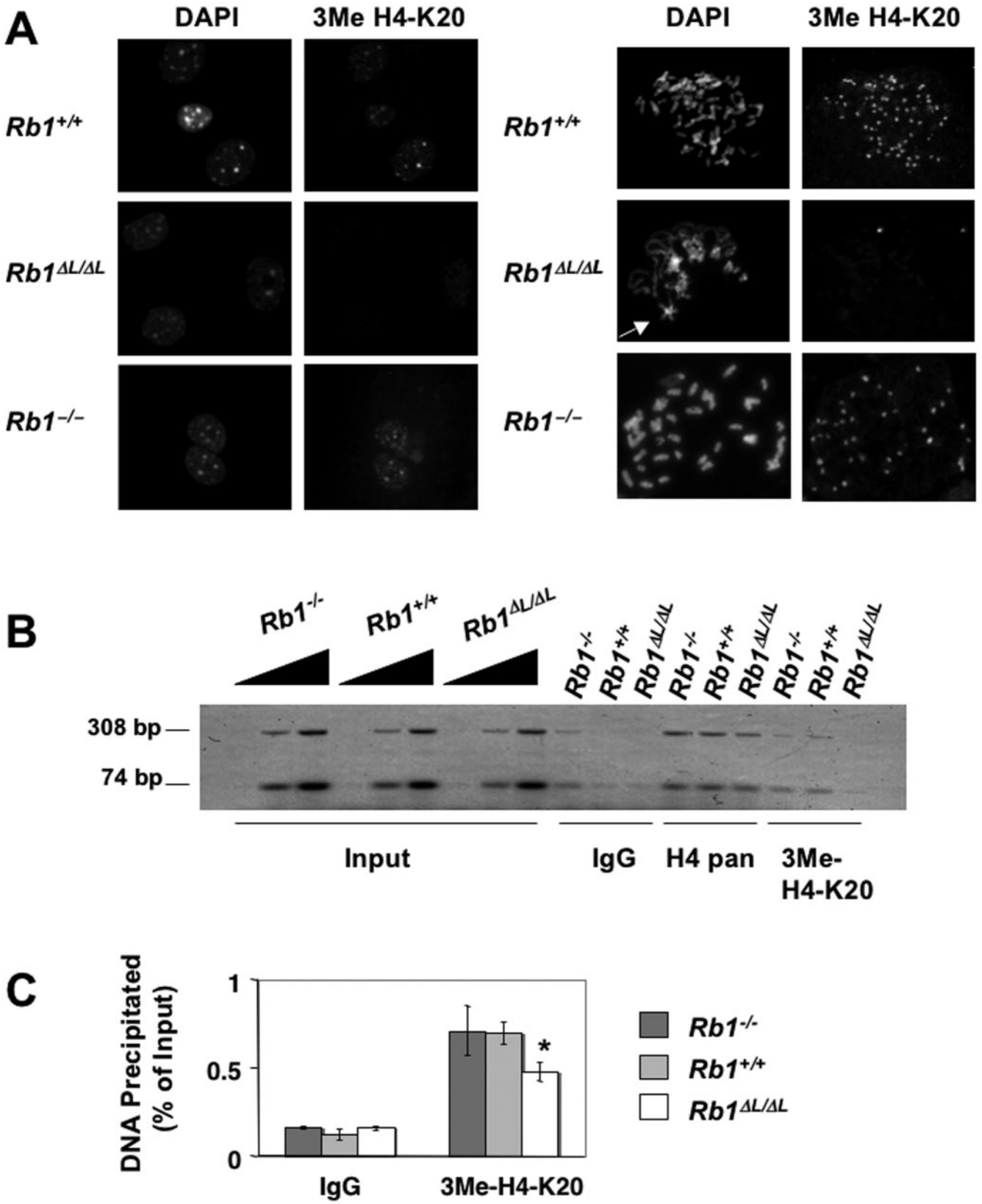

FIG. 7. Altered pericentric heterochromatin in $Rb1^{\Delta L/\Delta L}$ fibroblasts. (A) Representative fluorescent micrographs of interphase nuclei stained with DAPI and antibodies against trimethylated H4-K20 are shown in the left column. Similarly stained unfixed chromosome spreads for wild-type, $Rb1^{\Delta L/\Delta L}$, and $Rb1^{-/-}$ are shown on the right. The arrow indicates joined centromeres. (B) Chromatin immunoprecipitations were performed using the antibodies indicated below the gel. Major satellite repeat sequences were PCR amplified and analyzed by ethidium bromide staining of an

shown). This suggests that pRb is involved in regulating H4-K20 trimethylation primarily at pericentric heterochromatin and is less important elsewhere in the genome. However, our Western blots were unlikely to detect subtle reductions in the total level of this histone modification, and so we cannot rule out the existence of some changes outside of pericentric heterochromatin. Overall, our experiments provide multiple lines of evidence to support the conclusion that H4-K20 trimethylation in pericentric heterochromatin of $Rb1^{\Delta L/\Delta L}$ fibroblasts is reduced.

DISCUSSION

The LXCXE binding cleft is one of the most highly conserved structural features on the surface of pRb (33). This binding site is needed for viral oncoproteins to inactivate pRb, but it is also the natural binding site for a variety of cellular proteins. Using this site, pRb has been proposed to recruit a variety of chromatin regulators and to use them for a variety of cellular functions. This report examines the role of the LXCXE binding site in cell cycle control. Although pRb has been studied primarily for its role in the G_1/S transition, our experiments show that $Rb1^{\Delta L/\Delta L}$ cells lack some of the G_1/S-phase defects that are a feature of $Rb1^{-/-}$ cells. Contacts through this binding site do not appear to limit S-phase entry in actively proliferating cells. Potentially, pRb-mediated repression may be more important during cell cycle exit. $Rb1^{-/-}$ MEFs are unable to arrest in response to exogenous signals, like DNA damage (23) or transforming growth factor β1 (26), or drugs, like methotrexate (2) and MEK kinase inhibitors (9). In the future, it will be interesting to determine if any growth-regulating pathways controlled by these agents are affected in $Rb1^{\Delta L/\Delta L}$ fibroblasts.

Unexpectedly, mutation of the pRb-LXCXE binding site caused a defect in progression through mitosis, a defect that was characterized by lagging chromosomes during anaphase. Although the complete inactivation of pRb has recently been shown to cause defects in mitosis, $Rb1^{\Delta L/\Delta L}$ cells lack the upregulation of Mad2 that was reported to be responsible for this phenotype (24). Instead, our experiments reveal that the LXCXE binding site of pRb is specifically required for H4-K20 trimethylation at pericentric heterochromatin. When this histone modification is reduced, heterochromatin structure is altered. Presumably, this allows chromosomes to fuse in metaphase and causes them to lag in anaphase. The aneuploid cells seen by flow cytometry in Fig. 4B most likely resulted from missegregation of chromosomes or exit from a stalled mitosis without cytokinesis.

H4-K20 trimethylation defects in $Rb1^{\Delta L/\Delta L}$ cells are surprising, because this phenotype was previously shown to be a specific characteristic of cells lacking all three pRb family members and not to be present in cells that are null for individual pocket proteins, or even in double-null cells (20). Why, then, does this defect occur in $Rb1^{\Delta L/\Delta L}$ cells? One possible explanation is that the $Rb1^{\Delta L}$ allele is dominant and the mutant protein interferes with p107 and p130, preventing them from carrying out a function that is shared by all three family members. We think that this explanation is unlikely to be correct, because $Rb1^{\Delta L/\Delta L}$ cells do not display the other distinctive features of triple-knockout cells (data not shown). Fibroblasts deficient for all pocket proteins fail to respond to serum deprivation, lose viability upon contact inhibition, and fail to enter passage-induced senescence (10, 46). An alternative explanation, which we favor, is that pericentric H4-K20 trimethylation is singularly controlled by pRb under normal circumstances and this function is dependent on pRb's LXCXE binding cleft. In the complete absence of pRb, other family members assume this role, aided, perhaps, by the upregulation of p107 that occurs when pRb expression is lost. However, in $Rb1^{\Delta L/\Delta L}$ cells, this compensation does not seem to occur, because the expression of p107 or p130 does not increase in $Rb1^{\Delta L/\Delta L}$ fibroblasts (Fig. 2A). Also, the presence of the mutant protein may prevent other family members from substituting for pRb. Based on these arguments and the fact that p107 and p130 are exported from the nucleus in S phase (56), when H4-K20 trimethylation occurs, we conclude that pRb primarily controls this histone modification. Furthermore, with regard to this particular aspect of pRb function (regulation of H4-K20 trimethylation), our studies of the $Rb1^{\Delta L}$ mutant allele are more informative than the null allele.

The reestablishment of pericentric heterochromatin immediately following the replication of major satellite sequences is an area of active investigation (16, 57). Newly synthesized DNA is packaged with a mixture of older histones that contain the preexisting heterochromatin marks, along with newly synthesized histones. The mechanisms that mark newly replicated major satellite sequences are not well understood (16); however, nucleocatalytic assays have shown that H4 methylation occurs primarily in late S phase (42). Regardless of how heterochromatin is propagated, its conservation implies that trimethylation of H4-K20 by Suv4-20h enzymes occurs in every S phase to ensure faithful distribution of chromosomes in the ensuing mitosis. Extensive assembly of pericentric heterochromatin occurs in $Rb1^{\Delta L/\Delta L}$ cells, as evidenced by the fact that H3-K9 trimethylation and H3-K27 monomethylation remain intact (data not shown). H4-K20 trimethylation has been shown to be a relatively late step in the assembly of pericentric heterochromatin (48), suggesting that pRb plays a very specific role in regulating this histone modification. As pRb is known to be phosphorylated and inactive by this stage of the cell cycle, it is hard to envision how it directs the modification.

We envision two general possibilities to explain pRb's involvement in an S-phase event. The first is that, early in the cell cycle, pRb uses chromatin regulators to control expression of a gene whose product acts later in the cell cycle to control Suv4-20h trimethylation of H4-K20. Gonzalo et al. suggested that this regulation is unlikely to be mediated by E2F repression, because a dominant-negative E2F mutant that disrupts tran-

agarose gel (a negative image of the gel is shown). PCR amplification of these repeats generated both the 74-bp and 308-bp bands. Labels above each gel lane indicate the genotype of chromatin used for that lane. IgG, immunoglobulin G. (C) Major satellite sequences in precipitated chromatin were also analyzed by real-time PCR to quantify differences between wild-type, $Rb1^{-/-}$, and $Rb1^{\Delta L/\Delta L}$. The error bars indicate 1 standard deviation from the mean. The asterisk indicates a statistically significant difference (t test; $P < 0.001$).

scriptional control is unable to recapitulate the loss of H4-K20 trimethylation when expressed in wild-type MEFs (20). An alternative explanation is that while E2Fs have been shown to bind preferentially to underphosphorylated pRb (15), other interactions may be insensitive to pRb phosphorylation and persist through S phase. It has also been suggested that a small proportion of pRb remains active and localized to chromatin during S phase (4, 58). Thus, pRb may retain the ability to interact with Suv4-20h enzymes during S phase to regulate H4-K20 trimethylation. In previous work, all members of the pocket protein family have been shown to be capable of binding to Suv4-20h enzymes in vitro (20). However, p107 and p130 are known to be exported from the nucleus at the start of S phase (56). This may suggest why our experiments revealed that this modification is controlled primarily by pRb, as the other pocket proteins are not present in the nucleus when this histone modification is established. While pRb is able to bind directly to Suv4-20h proteins (Fig. 2D), it remains to be determined how LXCXE interactions may be involved in the regulation of H4-K20 trimethylation, since the $Rb1^{\Delta L}$ mutations have no effect on the pRb–Suv4-20h interaction. The structure of pRb includes two cyclin folds (33), and the LXCXE binding cleft of pRb is structurally analogous to the groove used by cyclins to interact with the PSTAIRE motif on cdks. In cdk regulation, this interaction is necessary for catalytic activity (29), as well as to guide substrate recognition (49), so it is appealing to speculate that pRb may play a similar role in activating catalysis or facilitating substrate recognition during histone methylation. Since $pRb^{\Delta L}$ can still interact with Suv4-20h enzymes, it is unlikely that Suv4-20h1 or -2 has an LXCXE motif that plays a role analogous to that of the PSTAIRE helix of cdks. We speculate that the LXCXE cleft on pRb most likely mediates substrate recognition or interacts with an additional factor that in turn activates Suv4-20h activity.

Considering how adversely these heterochromatin defects affect proliferating populations of fibroblasts, it is surprising that $Rb1^{\Delta L/\Delta L}$ mice are viable. In addition to studying fibroblast cultures, we have also examined mature tissues for evidence of these defects. Since H4-K20 trimethylation is absent in quiescent cells (5), we have investigated this modification in the thymus, where thymocytes are known to proliferate reliably. Surprisingly, we were unable to find aneuploid or tetraploid cells by flow cytometry of disaggregated thymocytes (data not shown). In addition, immunostaining revealed that only a small percentage of wild-type thymocytes have readily detectable H4-K20 trimethylation (data not shown). These experiments may suggest that endogenous proliferation rates are not sufficient to generate aneuploid cells faster than they can be eliminated, and thus, the mitotic defects in $Rb1^{\Delta L/\Delta L}$ fibroblasts are unable to be readily observed in vivo. This could mean that the $Rb1^{\Delta L/\Delta L}$ mitotic defect will generate genomic instability and lead to tumorigenesis in combination with other mutations that either accelerate cell proliferation or inhibit apoptosis. Experiments to investigate these possibilities are under way.

Intriguingly, a study of histone tail modifications that are altered in cancer cells found that H4-K20 trimethylation is ubiquitously reduced in lymphomas and colon carcinomas (17). Such a high frequency suggests that this change may contribute to the etiology of cancer and is not merely a by-product. Conceivably, pRb regulation of H4-K20 trimethylation may play an epigenetic role in tumor suppression. If human cells have similar compensatory mechanisms for the loss of pRb, the different properties of $Rb1^{\Delta L/\Delta L}$ and $Rb1^{-/-}$ MEFs raises the possibility that the loss of H4-K20 trimethylation may be a marker for the functional inactivation of pRb rather than its complete loss. Taken together with the data of Fraga et al. (17), our study reveals an intriguing connection between cancer genetics and epigenetics.

ACKNOWLEDGMENTS

We thank numerous investigators for reagents and advice during the course of this study: A. McClatchey, E. Li, S. Mittnacht, M. Classen, B. Kaelin, E. Hernando, C. Cordon-Cardo, T. Jenuwein, R. Bremner, and G. DiMattia. Many thanks to M. Keeney and W. Brown for expert assistance in flow cytometry and to J. Seabrook for help with statistical analysis. We gratefully acknowledge the advice of many colleagues at the MGH Cancer Centre, Dana-Farber, and the London Regional Cancer Program that helped to make this research possible.

C.E.I., S.M.F., L.A.S., and L.M.J. have all received support from the Strategic Training Program in Cancer Research. L.A.S. and S.M.F. also acknowledge funding from OGSST. N.G.B. is a recipient of a CIHR New Investigator Award. F.A.D. is a Research Scientist of the Canadian Cancer Society through an award from the National Cancer Institute of Canada. This work was supported by grants from the National Institutes of Health to N.J.D. (CA64402) and to L.H. (AG024398) and from the Canadian Institutes of Health Research to F.A.D. (MOP64253).

REFERENCES

1. **Aagaard, L., G. Laible, P. Selenko, M. Schmid, R. Dorn, G. Schotta, S. Kuhfittig, A. Wolf, A. Lebersorger, P. B. Singh, G. Reuter, and T. Jenuwein.** 1999. Functional mammalian homologues of the *Drosophila* PEV-modifier Su(var)3-9 encode centromere-associated proteins which complex with the heterochromatin component M31. EMBO J. **18:**1923–1938.
2. **Almasan, A., Y. Yin, R. E. Kelly, E. Y. Lee, A. Bradley, W. Li, J. R. Bertino, and G. M. Wahl.** 1995. Deficiency of retinoblastoma protein leads to inappropriate S-phase entry, activation of E2F-responsive genes, and apoptosis. Proc. Natl. Acad. Sci. USA **92:**5436–5440.
3. **Aparicio, O., J. V. Geisberg, E. Sekinger, E. Yang, Z. Moqtaderi, and K. Struhl.** 2005. Chromatin immunoprecipitation for determining the association of proteins with specific genomic sequences in vivo, p. 21.3.1–21.3.33. *In* F. M. Ausubel, R. Brent, R. E. Kington, D. D. Moore, J. G. Seidman, J. A. Smith, and K. E. Struhl (ed.), Current protocols in molecular biology. Greene Publishing Associates and Wiley-Interscience, New York, N.Y.
4. **Avni, D., H. Yang. F. Martelli, F. Hofmann, W. M. ElShamy, S. Ganesan, R. Scully, and D. M. Livingston.** 2003. Active localization of the retinoblastoma protein in chromatin and its response to S phase DNA damage. Mol. Cell **12:**735–746.
5. **Baxter, J., S. Sauer, A. Peters, R. John, R. Williams, M. L. Caparros, K. Arney, A. Otte, T. Jenuwein, M. Merkenschlager, and A. G. Fisher.** 2004. Histone hypomethylation is an indicator of epigenetic plasticity in quiescent lymphocytes. EMBO J. **23:**4462–4472.
6. **Blasco, M. A.** 2005. Mice with bad ends: mouse models for the study of telomeres and telomerase in cancer and aging. EMBO J. **24:**1095–1103.
7. **Brehm, A., E. A. Miska, D. J. McCance, J. L. Reid, A. J. Bannister, and T. Kouzarides.** 1998. Retinoblastoma protein recruits histone deacetylase to repress transcription. Nature **391:**597–601.
8. **Classon, M., S. R. Salama, C. Gorka, R. Mulloy, P. Braun, and E. E. Harlow.** 2000. Combinatorial roles for pRB, p107 and p130 in E2F-mediated cell cycle control. Proc. Natl. Acad. Sci. USA **97:**10820–10825.
9. **D'Abaco, G. M., S. Hooper, H. Paterson, and C. J. Marshall.** 2002. Loss of Rb overrides the requirement for ERK activity for cell proliferation. J. Cell Sci. **115:**4607–4616.
10. **Dannenberg, J.-H., A. van Rossum, L. Schuijff, and H. te Riele.** 2000. Ablation of the retinoblastoma gene family deregulates G1 control causing immortalization and increased cell turnover under growth-restricting conditions. Genes Dev. **14:**3051–3064.
11. **Dick, F. A., and N. Dyson.** 2002. Three regions of the pRB pocket domain affect its inactivation by human papillomavirus E7 proteins. J. Virol. **76:**6224–6234.
12. **Dick, F. A., E. Sailhamer, and N. J. Dyson.** 2000. Mutagenesis of the pRB pocket domain reveals that cell cycle arrest functions are separable from binding to viral oncoproteins. Mol. Cell. Biol. **20:**3715–3727.
13. **Dorin, J. R., E. Emslie, D. Hanratty, M. Farrall, J. Gosden, and D. J.**

Porteous. 1992. Gene targeting for somatic cell manipulation: rapid analysis of reduced chromosome hybrids by Alu-PCR fingerprinting and chromosome painting. Hum. Mol. Genet. **1:**53–59.
14. **Dunaief, J. L., B. E. Strober, S. Guha, P. A. Khavari, K. Alin, J. Luban, M. Begemann, G. R. Crabtree, and S. P. Goff.** 1994. The retinoblastoma protein and BRG1 form a complex and cooperate to induce cell cycle arrest. Cell **79:**119–130.
15. **Dyson, N.** 1998. The regulation of E2F by pRB-family proteins. Genes Dev. **12:**2245–2262.
16. **Ehrenhofer-Murray, A. E.** 2004. Chromatin dynamics at DNA replication, transcription and repair. Eur. J. Biochem. **271:**2335–2349.
17. **Fraga, M. F., E. Ballestar, A. Villar-Garea, M. Boix-Chornet, J. Espada, G. Schotta, T. Bonaldi, C. Haydon, S. Ropero, K. Petrie, N. G. Iyer, A. Perez-Rosado, E. Calvo, J. A. Lopez, A. Cano, M. J. Calasanz, D. Colomer, M. A. Piris, N. Ahn, A. Imhof, C. Caldas, T. Jenuwein, and M. Esteller.** 2005. Loss of acetylation at Lys16 and trimethylation at Lys20 of histone H4 is a common hallmark of human cancer. Nat. Genet. **37:**391–400.
18. **Frolov, M. V., D. S. Huen, O. Stevaux, D. Dimova, K. Balczarek-Strang, M. Elsdon, and N. J. Dyson.** 2001. Functional antagonism between E2F family members. Genes Dev. **15:**2146–2160.
19. **Garcia-Cao, M., S. Gonzalo, D. Dean, and M. A. Blasco.** 2002. A role for the Rb family of proteins in controlling telomere length. Nat. Genet. **32:**415–419.
20. **Gonzalo, S., M. Garcia-Cao, M. F. Fraga, G. Schotta, A. H. Peters, S. E. Cotter, R. Eguia, D. C. Dean, M. Esteller, T. Jenuwein, and M. A. Blasco.** 2005. Role of the RB1 family in stabilizing histone methylation at constitutive heterochromatin. Nat. Cell Biol. **7:**420–428.
21. **Hanahan, D., and R. A. Weinberg.** 2000. The hallmarks of cancer. Cell **100:**57–70.
22. **Harbour, J. W., and D. C. Dean.** 2000. The Rb/E2F pathway: expanding roles and emerging paradigms. Genes Dev. **14:**2393–2409.
23. **Harrington, E. A., J. L. Bruce, E. Harlow, and N. Dyson.** 1998. pRB plays an essential role in cell cycle arrest induced by DNA damage. Proc. Natl. Acad. Sci. USA **95:**11945–11950.
24. **Hernando, E., Z. Nahle, G. Juan, E. Diaz-Rodriguez, M. Alaminos, M. Hemann, L. Michel, V. Mittal, W. Gerald, R. Benezra, S. W. Lowe, and C. Cordon-Cardo.** 2004. Rb inactivation promotes genomic instability by uncoupling cell cycle progression from mitotic control. Nature **430:**797–802.
25. **Herrera, E., E. Samper, J. Martin-Caballero, J. M. Flores, H. W. Lee, and M. A. Blasco.** 1999. Disease states associated with telomerase deficiency appear earlier in mice with short telomeres. EMBO J. **18:**2950–2960.
26. **Herrera, R. E., T. P. Makela, and R. A. Weinberg.** 1996. TGFB-induced growth inhibition in primary fibroblasts requires the retinoblastoma protein. Mol. Biol. Cell **7:**1335–1342.
27. **Herrera, R. E., V. P. Sah, B. O. Williams, T. P. Makela, R. A. Weinberg, and T. Jacks.** 1996. Altered cell cycle kinetics, gene expression, and G_1 restriction point regulation in Rb-deficient fibroblasts. Mol. Cell. Biol. **16:**2402–2407.
28. **Hurford, R., D. Cobrinik, M.-H. Lee, and N. Dyson.** 1997. pRB and p107/p130 are required for the regulated expression of different sets of E2F responsive genes. Genes Dev. **11:**1447–1463.
29. **Jeffrey, P. D., A. A. Russo, K. Polyak, E. Gibbs, J. Hurwitz, J. Massague, and N. P. Pavletich.** 1995. Mechanism of CDK activation revealed by the structure of a cyclin A-CDK2 complex. Nature **376:**313–320.
30. **Jenuwein, T., and C. D. Allis.** 2001. Translating the histone code. Science **293:**1074–1080.
31. **Jorgensen, P., and M. Tyers.** 2004. How cells coordinate growth and division. Curr. Biol. **14:**R1014–R1027.
32. **Lakso, M., J. G. Pichel, J. R. Gorman, B. Sauer, Y. Okamoto, E. Lee, F. W. Alt, and H. Westphal.** 1996. Efficient in vivo manipulation of mouse genomic sequences at the zygote stage. Proc. Natl. Acad. Sci. USA **93:**5860–5865.
33. **Lee, J.-O., A. A. Russo, and N. P. Pavletich.** 1998. Structure of the retinoblastoma tumour-suppressor pocket domain bound to a peptide from HPV E7. Nature **391:**859–865.
34. **Lehnertz, B., Y. Ueda, A. A. Derijck, U. Braunschweig, L. Perez-Burgos, S. Kubicek, T. Chen, E. Li, T. Jenuwein, and A. H. Peters.** 2003. Suv39h-mediated histone H3 lysine 9 methylation directs DNA methylation to major satellite repeats at pericentric heterochromatin. Curr. Biol. **13:**1192–1200.
35. **Luo, R. X., A. A. Postigo, and D. C. Dean.** 1998. Rb interacts with histone deacetylase to repress transcription. Cell **92:**463–473.
36. **Magnaghi, L., R. Groisman, I. Naguibneva, P. Robin, S. Lorain, J. P. Le Villain, F. Troalen, D. Trouche, and A. Harel-Bellan.** 1998. Retinoblastoma protein represses transcription by recruiting a histone deacetylase. Nature **391:**601–604.
37. **Morris, E. J., and N. J. Dyson.** 2001. Retinoblastoma protein partners. Adv. Cancer Res. **82:**1–54.
38. **Näär, A. M., D. J. Taatjes, W. Zhai, E. Nogales, and R. Tjian.** 2002. Human CRSP interacts with RNA polymerase II CTD and adopts a specific CTD-bound conformation. Genes Dev. **16:**1339–1344.
39. **Niculescu, A. B., III, X. Chen, M. Smeets, L. Hengst, C. Prives, and S. I. Reed.** 1998. Effects of p21 Cip1/Waf1 at both the G_1/S and the G_2/M cell cycle transitions: pRb is a critical determinant in blocking DNA replication and in preventing endoreduplication. Mol. Cell. Biol. **18:**629–643.
40. **Nielsen, S. J., R. Schneider, U. M. Bauer, A. J. Bannister, A. Morrison, D. O'Carroll, R. Firestein, M. Cleary, T. Jenuwein, R. E. Herrera, and T. Kouzarides.** 2001. Rb targets histone H3 methylation and HP1 to promoters. Nature **412:**561–565.
41. **Peters, A. H., S. Kubicek, K. Mechtler, R. J. O'Sullivan, A. A. Derijck, L. Perez-Burgos, A. Kohlmaier, S. Opravil, M. Tachibana, Y. Shinkai, J. H. Martens, and T. Jenuwein.** 2003. Partitioning and plasticity of repressive histone methylation states in mammalian chromatin. Mol. Cell **12:**1577–1589.
42. **Rice, J. C., K. Nishioka, K. Sarma, R. Steward, D. Reinberg, and C. D. Allis.** 2002. Mitotic-specific methylation of histone H4 Lys 20 follows increased PR-Set7 expression and its localization to mitotic chromosomes. Genes Dev. **16:**2225–2230.
43. **Rieder, C. L., and H. Maiato.** 2004. Stuck in division or passing through: what happens when cells cannot satisfy the spindle assembly checkpoint. Dev. Cell. **7:**637–651.
44. **Robertson, K. D., S. Ait-Si-Ali, T. Yokochi, P. A. Wade, P. L. Jones, and A. P. Wolffe.** 2000. DNMT1 forms a complex with Rb, E2F1 and HDAC1 and represses transcription from E2F-responsive promoters. Nat. Genet. **25:**338–342.
45. **Sage, J., A. L. Miller, P. A. Perez-Mancera, J. M. Wysocki, and T. Jacks.** 2003. Acute mutation of retinoblastoma gene function is sufficient for cell cycle re-entry. Nature **424:**223–228.
46. **Sage, J., G. Mulligan, L. Attardi, A. Miller, S. Chen, B. Williams, E. Theodorou, and T. Jacks.** 2000. Targeted disruption of the three Rb-related genes leads to loss of G_1 control and immortalization. Genes Dev. **14:**3037–3050.
47. **Schneider, J. W., W. Gu, L. Zhu, V. Mahdavi, and B. Nadal-Ginard.** 1994. Reversal of terminal differentiation mediated by p107 in $Rb^{-/-}$ muscle cells. Science **264:**1467–1471.
48. **Schotta, G., M. Lachner, K. Sarma, A. Ebert, R. Sengupta, G. Reuter, D. Reinberg, and T. Jenuwein.** 2004. A silencing pathway to induce H3-K9 and H4-K20 trimethylation at constitutive heterochromatin. Genes Dev. **18:**1251–1262.
49. **Schulman, B. A., D. L. Lindstrom, and E. Harlow.** 1998. Substrate recruitment to cyclin-dependent kinase 2 by a multipurpose docking site on cyclin A. Proc. Natl. Acad. Sci. USA **95:**10453–10458.
50. **Sherr, C. J., and F. McCormick.** 2002. The RB and p53 pathways in cancer. Cancer Cell **2:**103–112.
51. **Sherr, C. J., and J. M. Roberts.** 2004. Living with or without cyclins and cyclin-dependent kinases. Genes Dev. **18:**2699–2711.
52. **Sicinski, P., J. L. Donaher, S. B. Parker, T. Li, A. Fazeli, H. Gardner, S. Z. Haslam, R. T. Bronson, S. Elledge, and R. A. Weinberg.** 1995. Cyclin D1 provides a link between development and oncogenesis in the retina and breast. Cell **82:**621–630.
53. **Stevaux, O., and N. J. Dyson.** 2002. A revised picture of the E2F transcriptional network and RB function. Curr. Opin. Cell Biol. **14:**684–691.
54. **Strober, B. E., J. L. Dunaief, S. Guha, and S. P. Goff.** 1996. Functional Interactions between the hBrm/hBRG1 transcriptional activators and the pRB family of proteins. Mol. Cell. Biol. **16:**1576–1583.
55. **Taylor, W. R.** 2004. FACS-based detection of phosphorylated histone H3 for the quantitation of mitotic cells. Methods Mol. Biol. **281:**293–299.
56. **Verona, R., K. Moberg, S. Estes, M. Starz, J. P. Vernon, and J. A. Lees.** 1997. E2F activity is regulated by cell cycle-dependent changes in subcellular localization. Mol. Cell. Biol. **17:**7268–7282.
57. **Verreault, A.** 2000. De novo nucleosome assembly: new pieces in an old puzzle. Genes Dev. **14:**1430–1438.
58. **Wells, J., P. S. Yan, M. Cechvala, T. Huang, and P. J. Farnham.** 2003. Identification of novel pRb binding sites using CpG microarrays suggests that E2F recruits pRb to specific genomic sites during S phase. Oncogene **22:**1445–1460.
59. **Zhao, J., B. K. Kennedy, B. D. Lawrence, D. A. Barbie, A. G. Matera, J. A. Fletcher, and E. Harlow.** 2000. NPAT links cyclin E-Cdk2 to the regulation of replication-dependent histone gene transcription. Genes Dev. **14:**2283–2297.
60. **Zijlmans, J. M., U. M. Martens, S. S. Poon, A. K. Raap, H. J. Tanke, R. K. Ward, and P. M. Lansdorp.** 1997. Telomeres in the mouse have large inter-chromosomal variations in the number of T2AG3 repeats. Proc. Natl. Acad. Sci. USA **94:**7423–7428.